Experimental and theoretical identification of adenine monolayers on Ag-terminated Si(111)

Luís M. A. Perdigão,[1] Paul A. Staniec,[1] Neil R. Champness,[2] R. E. A. Kelly,[3] L. N. Kantorovich,[3] and Peter H. Beton[1]

[1]*School of Physics and Astronomy, University of Nottingham, Nottingham NG7 2RD, United Kingdom*

[2]*School of Chemistry, University of Nottingham, Nottingham NG7 2RD, United Kingdom*

[3]*Department of Physics, School of Physical Sciences and Engineering, King's College London, Strand, London,*
WC2R 2LS, United Kingdom

We discuss the formation of ordered adenine monolayers on a Ag-Si(111)$\sqrt{3} \times \sqrt{3}R30°$ surface held at room temperature. Adenine forms a hexagonal network, which is stabilized by hydrogen bonding. By comparing the ordering observed using scanning tunneling microscopy with molecular superstructures calculated using *ab initio* density functional theory, we suggest that adenine forms an array of irregular hexagons through the combination of three distinct hydrogen-bonded adenine dimers. The dimensions of the ordered monolayer are commensurate with the surface with $\sqrt{3} \times \sqrt{7}$ periodicity relative to the Ag-Si(111)$\sqrt{3} \times \sqrt{3}R30°$ reconstruction, in agreement with calculated molecular dimensions. An analysis of double-domain regions leads us to conclude that there are two domains with different chiralities.

PACS number(s): 68.37.−d

The use of highly directional intermolecular interactions to control the organisation of adsorbed molecules has been attracting increasing attention in recent years. The formation of extended structures, such as rows and two-dimensional networks, has been demonstrated using a number of different interactions such as metal coordination, hydrogen bonding, and dipolar coupling.[1–11] It is well known that the structure of many complex biological structures is determined by intermolecular interactions—for example, hydrogen bonding—and this has motivated an investigation of the ordering of simple biomolecules such as nucleic acids and amino acids on a range of solid substrates.[12–19] Studies based on scanning tunneling microscopy (STM) have revealed that simple biomolecules may adopt many complex two-dimensional arrangements that are also controlled by hydrogen bonding.

When incorporated within DNA, adenine (Fig. 1) forms a double hydrogen bond with its complementary base, thymine. The monolayers formed by adenine when adsorbed on a surface have been studied by several different groups who have proposed a range of structures based on hydrogen bonding.[12–19] Adenine is reported to form large ordered networks and, in some cases, isolated chains. Furukawa *et al.*[12] reported the formation of double chains and hexagonal islands on Cu(111). In contrast, deposition on Cu(110) results in molecular chains along two possible directions with ordering which is determined in part by the surface-induced chirality of adenine.[13] This occurs since rotation about an axis lying in a plane parallel to the molecules, corresponding to flipping motion between the two states shown in Fig. 1, is suppressed for adsorbed molecules. The adsorption of adenine on a clean Si(100) surface has also been studied, where molecules are found to interact strongly with the Si dangling bonds.[18,19]

Adenine has also been the subject of a number of theoretical investigations.[12,13,15,20–23] It has recently been shown[20] that there are six inequivalent sites, referred to subsequently as binding sites, for hydrogen bonding around the edges of a single adenine molecule, resulting in 21 distinct configurations of adenine pairs bound by a double hydrogen bond. However, only a few combinations play a significant role in

the ordering of molecules on the surface since many configurations have low binding energy.

We report here a study of adenine adsorbed on an Ag-Si(111)$\sqrt{3} \times \sqrt{3}R30°$ surface at room temperature. We have chosen this substrate because a range of organic molecules are known to diffuse freely allowing the formation of self-assembled structures with the order predominantly determined by intermolecular interactions as opposed to molecule-substrate interactions.[7,10,24] Images acquired using STM were analyzed to determine the structure, commensurability, and growth of ordered monolayers. A model is proposed for the observed ordering which is supported by theoretical calculations based on density functional theory (DFT). We also demonstrate that the adenine domains are chiral and that both chiral domains are observed.

The deposition of adenine was performed under ultrahigh-vacuum (UHV) conditions (base pressure $<10^{-10}$ Torr). Ag-Si(111)$\sqrt{3} \times \sqrt{3}R30°$ surfaces were prepared using a two-step process consisting of an initial anneal up to ~ 1200 °C, followed by deposition of Ag while controlling the sample temperature at ~ 500 °C.[25] Adenine was deposited on the Ag-Si(111)$\sqrt{3} \times \sqrt{3}R30°$ surface by sublimation. Images of the surface were obtained using an STM housed within the UHV chamber, operated in constant-current mode at room temperature.

STM images acquired after exposing the surface to adenine (0.5 monolayer) show the formation of large islands
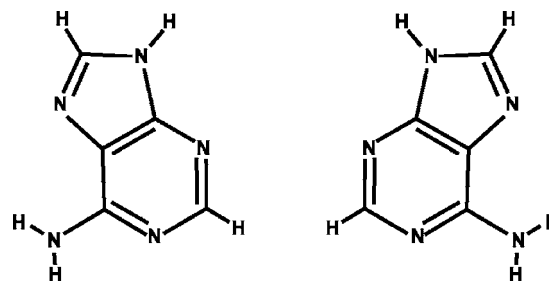
FIG. 1. Chemical structure of a single adenine molecule in two different planar configurations.
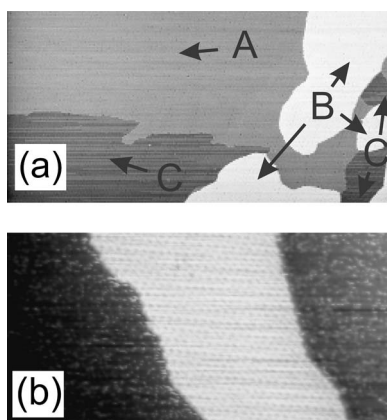
FIG. 2. (a) 5000 Å×2500 Å STM image of ∼0.5 monolayer of adenine on Ag-Si(111)$\sqrt{3}\times\sqrt{3}R30°$. Arrows indicate different regions: *A*: adenine structure. *B* and *C*: Ag-Si(111)$\sqrt{3}\times\sqrt{3}R30°$ surface with *B* a higher terrace. (b) 500 Å×250 Å STM image of an adenine island. The noise observed around the island is due to diffusing molecules. Feedback parameters for both images are −3.1 V, 50 pA.

[see Fig. 2(a)] with an apparent height of ∼1.2 Å. Our images were acquired with a sample voltage in the range between −2.7 V and −3.3 V. Outside this voltage range the STM scanning resulted in the disruption of the molecular islands. The formation of domains is an indication that, as expected, adenine diffuses readily on this surface at room temperature. Figure 2(b) shows a 500 Å×250 Å image of an elongated domain. A structure with hexagonal order can be identified, characterized by parallel rows of dimers along one direction. Figure 3 shows an image, obtained at −2.7 V sample bias, in which both the adenine and the Ag-Si(111)$\sqrt{3}\times\sqrt{3}R30°$ surface are resolved. The lattice constant *a* of the Ag-Si(111)$\sqrt{3}\times\sqrt{3}R30°$ surface is 6.65 Å, and from images such as these it is straightforward to determine the unit-cell dimensions of the adenine layer relative to the Ag-terminated Si(111) surface.

Figure 4(a) shows a close-up image of an adenine region with overlaid dark spots to indicate the positions of the low-
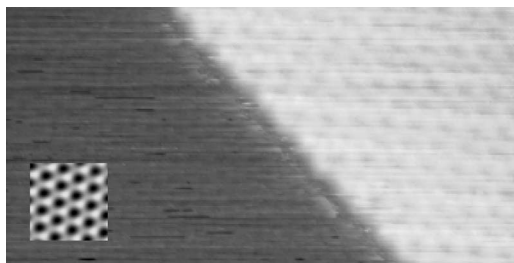
FIG. 3. 200 Å×100 Å STM image of an adenine domain (top right) and the $\sqrt{3}\times\sqrt{3}$ reconstruction of the Ag:Si(111) surface (bottom left). Feedback parameters −2.7 V, 50 pA. The main figure is an unfiltered image but we have also made use of filtered images in which the substrate detail is enhanced so that registry of the molecular overlayer with substrate may be identified (see Fig. 4). A small area (lower left hand corner) within the STM image has been overlaid by the same area of the same image after application of a fast Fourier transform filtering routine.
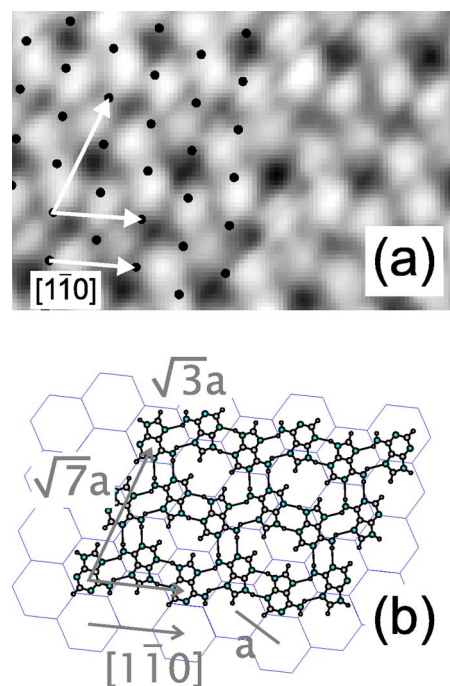
FIG. 4. (Color online) (a) 60 Å×40 Å image of the adenine structure from Fig. 3, where a low-pass filter was applied to remove high-frequency noise. The dark dots represent the position of low-contrast regions of the underlying Ag-Si(111)$\sqrt{3}\times\sqrt{3}R30°$ surface (see text). The arrows represent the unit-cell vectors for the periodicity observed. (b) Model proposed for adenine structure on the surface. Vertices and centers of the hexagons represent Ag trimers and Si trimers respectively. One of the [1$\bar{1}$0] directions of the Si substrate is also represented and *a*=6.65 Å is the lattice constant of the Ag-Si(111)$\sqrt{3}\times\sqrt{3}R30°$ surface.

contrast regions of the underlying Ag-Si(111)$\sqrt{3}\times\sqrt{3}R30°$, corresponding to Si trimers in the honeycomb chain trimer model for this surface.[26–28] As shown in Fig. 4(a) the position of the adenine molecules repeats periodically along the directions indicated by arrows. The dimensions of the adenine unit cell defined by the arrows in Fig. 4(a) are $\sqrt{3}a \times \sqrt{7}a$, or 11.5 Å×17.6 Å, and the angle between the unit cell vectors is 70.9°. Four lobes are resolved in the STM image of the unit cell, each of which corresponds to one adenine molecule. The images indicate that the four-molecule cell consists of two pairs of molecules which have a similar appearance in STM images but are inequivalent since they are adsorbed above different sites on the surface. We are careful at this stage not to rule out the possibility that the two molecular pairs could have slightly different configurations which are not directly imaged due to the resolution limitations of the STM.

There are many distinct configurations of adenine monolayers, which are stabilized by H bonding. We consider first a simple approach in which the adenine monolayer is formed from the most energetically favorable combinations of stabilized pairs which may be arranged in a two-dimensional network. The H-bonded dimers in Figs. 5(a)–5(c) have high stabilization energies,[20] making them good candidates to explain the structures observed in the STM images. Note that both DFT and less accurate semiempirical calculations[13] pre-
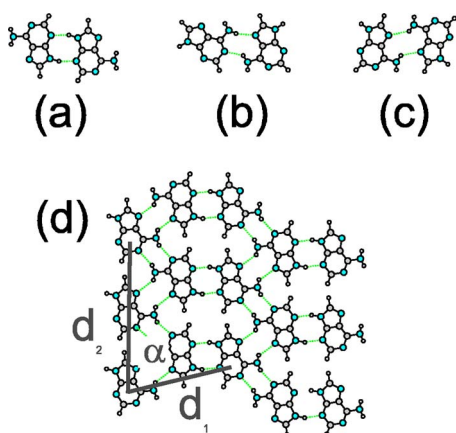
FIG. 5. (Color online) (a), (b), and (c) Molecular models of high-binding-energy adenine dimers (see text). Chains of dimers can be obtained by connecting consecutive (a) dimers by using a (b) hydrogen bonding configuration. Identical parallel chains can then form hydrogen bonds with each other using configuration (c) resulting in the structure represented in (d). d_1 and d_2 are distances between adenine molecules as shown, corresponding, respectively, to the $\sqrt{3}a$ and $\sqrt{7}a$ directions in Fig. 4.

dict that the dimer in Fig. 5(a) is the most stable pair.

Figure 5(d) shows a distorted hexagonal structure obtained by combining the three dimers identified in Figs. 5(a)–5(c). This model was also used in Fig. 4(b) for the suggested adenine structure. The suggested structure, as drawn in Fig. 5(d), contains only two molecules in the primitive cell, but when overlaid on the surface as in Fig. 4(b) adjacent hexagons sit above inequivalent sites, giving rise to a unit cell with four molecules. The distances d_1 and d_2 between molecules at equivalent sites on the surface are defined in Fig. 5(d). In Table I the values for d_1 and d_2 for the commensurate $\sqrt{3}a \times \sqrt{7}a$ structure are compared with calculated values in the literature for this molecular arrangement. Our experimental values agree very well with the values obtained from calculations by Kelly and Kantorovitch[22] and Shinoda *et al.*[21] with small differences of less than 0.4 Å. The small discrepancy in the distances can be explained by the fact that the hydrogen bonds compete with the stabilization provided by the adenine-surface interaction resulting in the commensurability observed.

Despite the close agreement between the dimensions of our proposed structure and the observed unit cell dimensions it is useful to systematically exclude all other possible arrangements.

TABLE I. Comparison of distances d_1 and d_2 [see Fig. 5(d)] and angle α between adenine dimers, determined experimentally (using the model of $\sqrt{3}a \times \sqrt{7}a$ periodicity) and calculated values obtained from the literature.

	d_1 (Å)	d_2 (Å)	α (deg)
$\sqrt{3}a \times \sqrt{7}a$ model	11.5	17.6	70.9
Shinoda *et al.*[a]	11.5	16.8	~75.5
Kelly and Kantorovich[b]	11.4	17.2	73.8

[a]Reference 21.
[b]Reference 22.
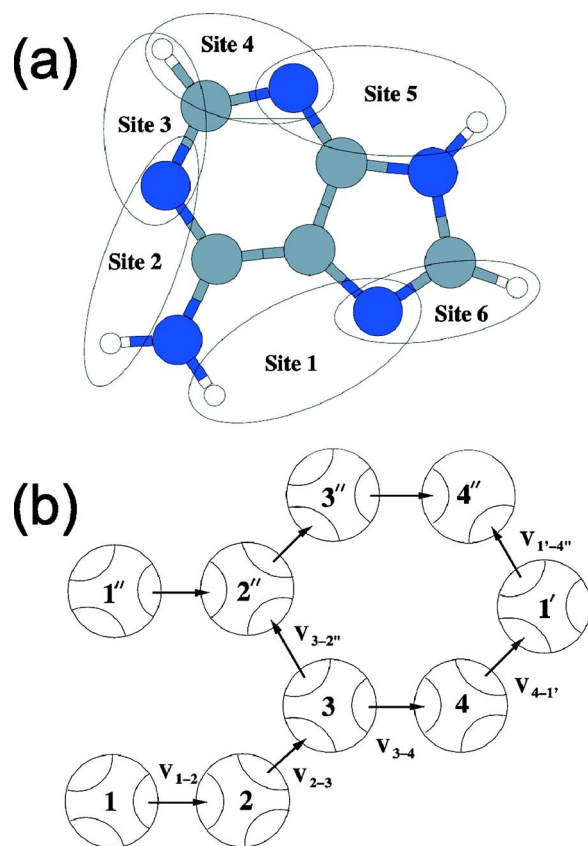
FIG. 6. (Color online) (a) Binding sites of a single adenine molecule. (b) Schematic of an adenine monolayer with four molecules in the unit cell. Like numbers correspond to equivalent molecules in different cells that are distinguished by single and double primes. The vectors shown connect the midpoints of the two binding sites in each dimer (Ref. 22).

rangements. As mentioned earlier, there are 21 possible hydrogen-bonded adenine pairs which result from hydrogen bonding between different sites on the molecule as shown schematically in Fig. 6. These may be combined, prior to the final atomic relaxation, to form all possible gas-phase (i.e., planar arrangements in the absence of a substrate) monolayers as suggested in Ref. 22 It is convenient for our discussion to consider an adenine repeat unit in which molecules are numbered 1–4 as shown in Fig. 6. In the method proposed in Ref. 22, *all* four-molecule cells (and thus all two-molecule cells as well) have been generated by incorporating adenine dimers in all possible ways into a chain 1-2-3-4, which serves as the primitive unit cell, and then considering all possible arrangements of the chains with respect to each other in the monolayer. In the gas phase 17 distinct monolayers with 2 molecules per unit cell and 1331 distinct structures for monolayers with 4 molecules per unit cell have been identified.

In order to find the structure (or structures) that correspond to the adenine monolayer observed in our STM experiments, we modified the methodology described above to generate all two- and four-molecule gas-phase cells with lattice constants close to the observed cell dimensions. This method is justified since the surface provides a periodic array

TABLE II. Calculated values for comparison with experimentally observed unit cell sizes d_1 and d_2 (see Table I) and stabilization energies for the gas-phase monolayers shown in the Appendix. Also tabulated are the binding energies in fully relaxed (E_1) and partially relaxed (E_2) monolayers in units of eV/molecule (see text). The relationship between the calculated primitive unit-cell dimensions d_1^* and d_2^* and the tabulated values of d_1 and d_2 is $d_1^* = d_1$ and $d_2^* = d_2/2$ for the two molecule primitive cells A2–D2; $d_1^* = d_1$ and $d_2^* = d_2$ for four molecule primitive cells $B4$, $H4$, and $I4$; $d_1^* = 2d_1$ and $d_2^* = d_2/2$ for four molecule unit cells $A4$, $C4$–$G4$. The site-site combinations for each adenine dimer along the chain within the cell and between adjacent parallel chains are indicated explicitly [see Fig. 6(a)]. Note that the values of E_2 for $E4$, $H4$, and $I4$ are missing because the partial relaxation resulted in structures strongly deviating from the required hexagonal network. Also note that $A2$, $A4$, and $B4$ were previously reported in Ref. 22; in the present study, the $A2$ structure was recalculated with a better precision.

Monolayer	Pairs along the chain				Pairs between chains		After relaxation				
	1-2	2-3	3-4	4-1'	1"-4"	3-2"	d_1 (Å)	d_2 (Å)	α (deg)	E_1 (eV per molecule)	E_2 (eV per molecule)
A2	5,5	1,1			2,2		11.4	17.2	73.7	−0.88	−0.87
B2	2,5	2,5			6,1		12.2	17.4	71.0	−0.78	−0.57
C2	2,2	5,5			6,6		12.2	19.4	70.6	−0.77	−0.13
D2	3,2	6,5			6,5		11.5	18.6	70.6	−0.62	−0.08
A4	5,5	1,2	5,5	2,1	2,1	1,2	11.9	17.0	69.0	−0.92	−0.72
B4	1,2	1,1	2,1	2,2	5,5	5,5	11.9	17.4	71.2	−0.85	−0.81
C4	5,5	1,2	5,2	5,1	2,6	1,2	11.8	17.6	71.1	−0.81	−0.75
D4	2,2	5,2	5,5	2,5	6,1	1,6	12.2	17.8	71.3	−0.77	−0.70
E4	2,2	5,2	5,2	5,5	6,6	1,6	12.2	19.0	70.7	−0.76	
F4	5,5	1,5	2,2	5,1	2,6	6,2	11.9	18.2	74.4	−0.75	−0.55
G4	1,2	6,6	2,1	3,3	5,5	5,5	12.4	19.6	63.2	−0.75	−0.45
H4	5,1	2,2	1,3	5,1	2,6	5,5	12.1	21.2	83.9	−0.73	
I4	5,1	2,5	6,3	5,1	2,6	5,2	12.2	22.4	91.5	−0.70	

of potential wells in which the molecules settle and in our calculation this effect is implicitly taken into account by using constrained unit cell sizes. Only monolayers with lattice vectors close to the experimental values were selected for consideration. More precisely we consider cells with lattice vectors with lengths in the range $d_1 = 11.5 \pm 1$ Å, $d_2 = 17.6 \pm 1$ Å, or multiples of these, and an angle between them, $\alpha = 70.9 \pm 10°$. We allow for some variance from the experimental dimensions to take account of the additional relaxation due to the molecule-surface interaction which is not included in our calculations. We find that only *four* arrangements with two molecules in the primitive cell have lattice vectors in the range specified above. Note that a unit cell with dimensions d_1 and d_2 as above contains two primitive two-molecule cells.

As stated above there are four molecules per unit cell in our STM images. We can account for this arrangement in terms of a two-molecule gas-phase primitive cell which is arranged on the surface such that alternate primitive cells are adsorbed above different surface sites. However, we also consider the alternative possibility that the gas-phase primitive cell has four molecules. In the case of four-molecule primitive cells, an additional constraint was applied that the two molecular pairs within the cell should have an orientation and position such that they could appear to be equivalent in STM images. More specifically, we selected only such cells in which the vectors connecting molecules 1-2 and 3-4 are approximately equal: $V_{12} \approx V_{34}$, $V_{23} \approx V_{14'}$, and $V_{32"} \approx V_{1'4"}$ (see Fig. 6), with no more than 1 Å difference in length and 15° in direction. Two possibilities occur with the actual lattice vectors of the primitive cell of the expected structures to be close to (i) 11.5 Å and 17.6 Å or (ii) 23.0 Å

and 8.8 Å. We found that only 17 four-molecule cells satisfy these conditions.[28]

From all 21 selected structures, 13 structures have been chosen that have the highest stabilization energies and for these both the atomic positions and the unit-cell dimensions were fully relaxed using a DFT method as implemented in the SIESTA code,[29–31] using periodic boundary conditions, norm-conserving pseudopotentials, and the Perdew-Becke-Ernzerhof (PBE) density functional.[32] In all our calculations we have used the DZP (double-zeta plus polarization) orbitals localized basis set [corresponding to the energy cutoff of 10 meV (Ref. 31)]. Since this basis set is not complete, the basis set superposition error (BSSE) correction[33] was applied to get reliable stabilization (binding) energies of the monolayers. Atomic relaxation was performed until the forces on atoms were less than 0.05 eV/Å. Due to large sizes of the supercells used in our calculations, only a single (gamma) point was utilized.

The resulting dimensions for the arrays following full relaxation are summarized in Table II including values for the predicted dimensions for unit cells with two and four molecules. Two new vectors d_1^* and d_2^* have been defined in our calculations for each monolayer. These vectors correspond to the calculated primitive cell vectors—both the vectors and molecular configurations are identified in the Appendix. Configuration $A2$, based on the two-molecule gas-phase cell, corresponds to the structure identified in Fig. 5(d) and has dimensions which are very close to those observed in our STM images. The three four-molecule cells $A4$, $B4$, and $C4$, also have cell dimensions close to experimental values. In all other cases the relaxed unit-cell dimensions are too large to be considered realistic candidates for the observed structures.

The structure $A2$ is the most energetically favorable among all two-molecule gas-phase structures, while the $A4$, $B4$, and $C4$ configurations are the three most favorable within the all four-molecule structures. However, on inspection of the molecular arrangement of $C4$ following relaxation we find that it violates the requirement (discussed above) that the molecular pairs making up the cell be sufficiently close in orientation to appear similar in STM images; therefore, this configuration is discarded. Thus, the three best candidates for the observed structure are $A2$, $A4$, and $B4$.

In our analysis above, the interaction of the surface with adenine molecules is neglected. Although it is possible to perform calculations which include atoms from the substrate, these require a large amount of processing power. Nevertheless, it is clear that the surface provides a set of periodic potential wells for the adenine molecules that constrains their arrangement in the monolayer, which can result in either an increase or reduction of the intermolecular distance with respect to the values in the gas-phase considered above. Since the repulsion between molecules increases more rapidly with the reduction of the intermolecular distance than the attraction with the increase of this distance, it is more likely that the separation between molecules would increase on the surface with respect to the gas phase. Our previous studies of adsorbed molecules on this surface also support this trend: we have observed arrays in which the intermolecular separation on the surface differs slightly from that in the bulk crystalline form (where these values are available) or the calculated gas phase separation.[34] However these differences correspond to increases in the surface lattice constant by up to $\sim$0.5 Å, while the largest reduction is less than 0.1 Å; i.e., the surface phases are much more susceptible to extension than compression. In Table II the only array in which both the calculated unit-cell dimensions are less than those observed in our images is configuration $A2$, providing strong evidence that this is the correct assignment for our observed structure.

In order to estimate the possible effect of the surface on the adenine monolayer, we performed a set of additional calculations in which the unit-cell dimensions were constrained to match exactly the experimental values, while all atoms of the adenine molecules were allowed to relax. The binding energies per molecule obtained under this constraint for all 13 selected monolayers are reported in the last column (E_2) of Table II. The difference between the binding energies E_2 and E_1, characterizes the loss in the monolayer energy due to expansion and contraction of the gas-phase lattice constants to match those of the surface phase. We see from our results that, apart from the structures $A2$ and $B4$ that lose only 0.02 eV and 0.04 eV, respectively, all other structures experience a much larger distortion. In particular, the other candidate structure $A4$ goes up by 0.20 eV in energy. If we assume that the energy gain due to adsorption on the surface is approximately the same for all the structures, we can clearly conclude that the $A2$ and $A4$ configurations would be the most energetically favorable structures, closely followed by the $B4$ structure. Finally we note that the molecular arrangements $A2$ and $B4$ we have invoked to explain our results have surface-induced chirality. This effect has previously been reported in Ref. 35 mentioned above. We have
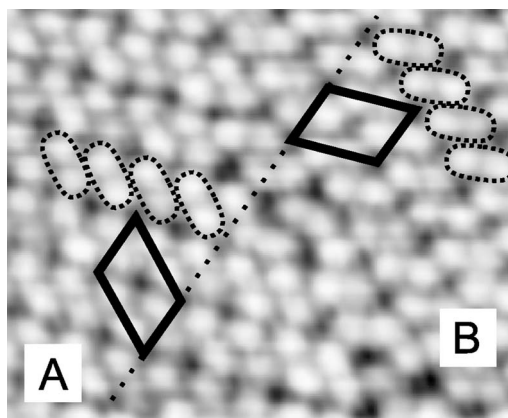
FIG. 7. 100 Å$\times$80 Å STM image of two separate domains A and B. A low-pass filter was applied from the original image in order to reduce noise. The $\sqrt{3}a \times \sqrt{7}a$ unit cells (containing four molecules) are shown in bold. The dotted line is the $\sqrt{3}a$ direction (corresponding to the $[1\bar{1}0]$ direction of the underlying surface), which is common in both domains (see Fig. 4). The rows of adenine dimers are also highlighted.

observed the same effects on our surface as is demonstrated in a high-resolution image in Fig. 7 where we find evidence of chirality. The repeating motif in the molecular array is the row of tilted dimers identified by ellipses in Fig. 7. It is simple to infer that the two domains A and B may be transformed into each other through reflection, but not rotation. The structure $A4$ is not chiral (i.e., is the same if flipped) and thus should be discarded. Although structure $B4$ observes all the requirements explained above, we note that single adenine molecules in consecutive rows of this structure alternate in chirality. We believe that if this structure had formed, it would clearly be visible in the STM images as alternating contrast rows. In addition for this structure we do not believe it would be possible to distinguish domains with opposite chirality such as observed in Fig. 7.

Overall our more detailed analysis strongly supports the assignment discussed above on the basis of simple physical arguments. The $A2$ structure suggested here for the Ag-Si(111)$\sqrt{3}\times\sqrt{3}R30°$ surface has already been proposed in Ref. 34 for the adenine adsorption on the molybdenite surface. The hexagonal structure proposed in Refs. 12, 16, and 23 is in fact our $A4$ structure that was dismissed above. The structure proposed by Tao and Shi for adenine adsorption on graphite[17] has very different cell dimensions from the ones observed here.

We have demonstrated that adenine forms well-ordered structures spontaneously when deposited onto a Ag-Si(111)$\sqrt{3}\times\sqrt{3}R30°$ surface. Only one phase was found, together with its chiral partner, which is stabilized by the formation of stable double hydrogen bonds between the adenine molecules. The structure was found to be commensurate with the surface with a $\sqrt{3}\times\sqrt{7}$ superstructure and dimensions in very good agreement with calculated values, although the exact registry with surface remains unresolved. Distinguishing which of the many possible adenine monolayers accounts for our observed structure relies on a combination of accurate calibration of our STM images using the

substrate lattice constant and the use of *ab initio* techniques to calculate accurate estimates of intermolecular spacings. We have also shown that larger cells as seen in the STM images may in some cases be required to propose appropriate atomistic models for the molecular networks.

APPENDIX

Selected adenine gas-phase monolayers are given in Fig. 8. $A2-D2$ are two molecule cells and $A-I4$ are four molecule cells. For each cell, vectors d_1^* and d_2^* are defined as shown. Each cell has been minimized as explained in the article. The calculated parameters d_1^*, d_2^*, angle, and energy for each of these primitive cells can be found in Table II.
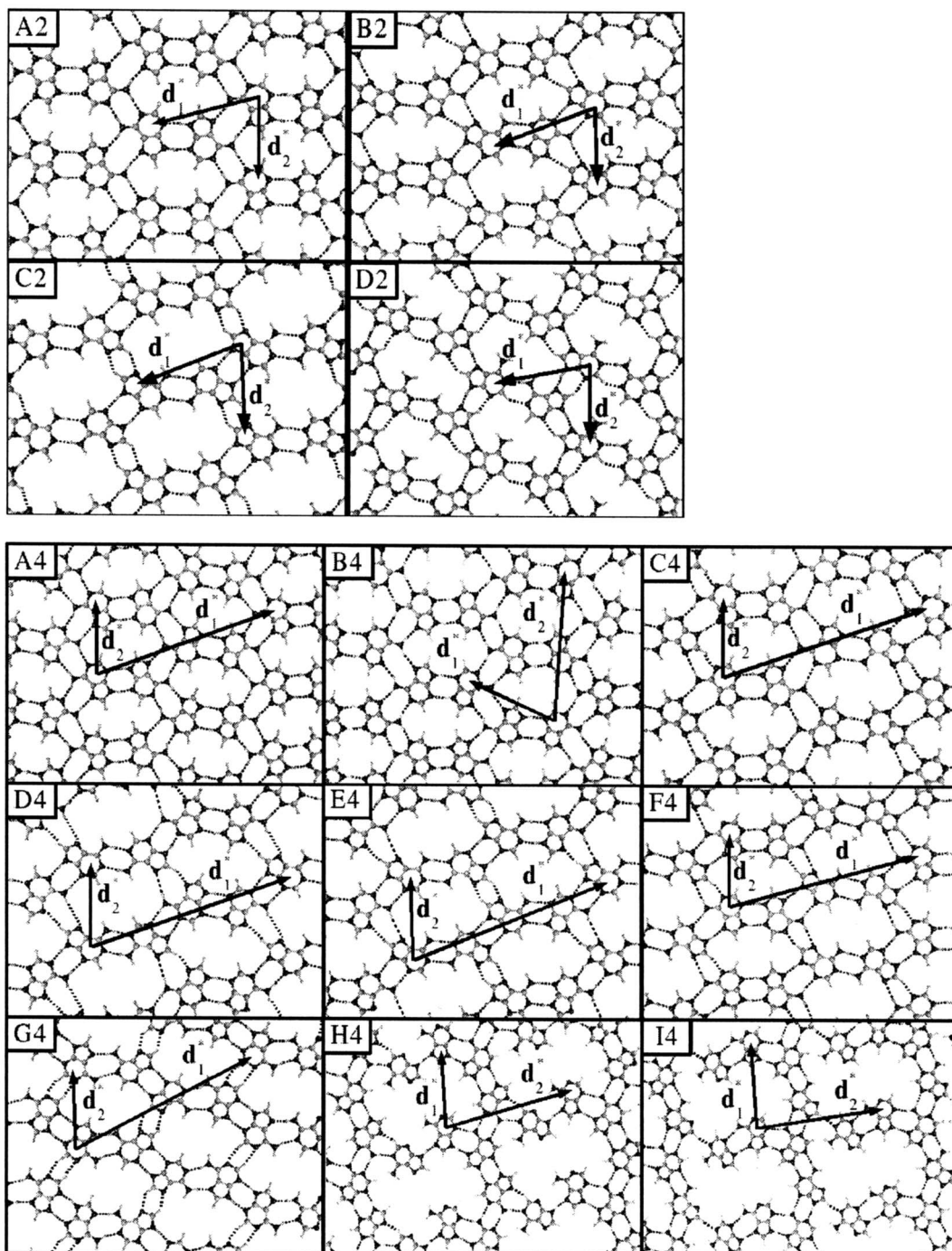
FIG. 8. Selected adenine gas-phase monolayers.

[1] S. Griessl, M. Lackinger, M. Edelwirth, M. Hietschold, and W. M. Heckl, Single Mol. **3**, 25 (2002).

[2] A. Dmitriev, N. Lin, J. Weckesser, J. V. Barth, and K. Kern, J. Phys. Chem. B **106**, 6907 (2002).

[3] S. D. Feyter and F. C. De Schryver, Chem. Soc. Rev. **32**, 139 (2003).

[4] C. Bobisch, Th. Wagner, A. Bannani, and R. Möller, J. Chem. Phys. **119**, 9804 (2003).

[5] T. Yokoyama, S. Yokoyama, T. Kamikado, Y. Okuno, and S. Mashiko, Nature (London) **413**, 619 (2001).

[6] J. V. Barth, J. Weckesser, C. Cai, P. Günter, L. Bürgi, O. Jeandupeux, and K. Kern, Angew. Chem., Int. Ed. **39**, 1230 (2000).

[7] D. L. Keeling, N. S. Oxtoby, C. Wilson, M. J. Humphry, N. R. Champness, and P. H. Beton, Nano Lett. **3**, 9 (2003).

[8] S. Feyter, A. Miura, S. Yao, Z. Chen, F. Würthner, P. Jonkheijm, A. P. H. J. Schenning, E. W. Meijer, and F. C. De Schryver, Nano Lett. **5**, 77 (2005).

[9] R. Otero, M. Schöck, L. M. Molina, E. Lœgsgaard, I. Stensgaard, B. Hammer, and F. Besenbacher, Angew. Chem. **117**, 2 (2005).

[10] J. A. Theobald, N. S. Oxtoby, M. A. Phillips, N. R. Champness, and P. H. Beton, Nature (London) **424**, 1029 (2003).

[11] M. T. Cuberes, R. R. Schlittler, and J. K. Gimzewski, Surf. Sci. **371**, L231 (1997).

[12] M. Furukawa, H. Tanaka, and T. Kawai, Surf. Sci. **445**, 1 (2000).

[13] Q. Chen, D. J. Frankel, and N. V. Richardson, Langmuir **18**, 3219 (2002).

[14] S. Sowerby, G. B. Petersen, and N. G. Holm, Origins Life Evol. Biosphere **32**, 35 (2002).

[15] S. J. Sowerby, M. Edelwirth, and W. M. Heckl, J. Phys. Chem. **102**, 5914 (1998).

[16] J. E. Freund, M. Edelwirth, P. Kröbel, and W. M. Heckl, Phys. Rev. B **55**, 5394 (1997).

[17] N. J. Tao and Z. Shi, J. Phys. Chem. **98**, 1464 (1994).

[18] M. Kasaya, H. Tabata, and T. Kawai, Surf. Sci. **342**, 215 (1995).

[19] M. Kasaya, H. Tabata, and T. Kaway, Surf. Sci. **357–358**, 195 (1996).

[20] R. E. A. Kelly, Y. J. Lee, and L. N. Kantorovich, J. Phys. Chem. B **109**, 11933 (2005).

[21] K. Shinoda, W. Shinoda, C. C. Liew, S. Tsuzuki, Y. Morikawa, and M. Mikami, Surf. Sci. **556**, 109 (2004).

[22] R. E. A. Kelly and L. N. Kantorovich, Surf. Sci. **589**, 139 (2005).

[23] S. Sowerby, P. A. Stockwell, W. M. Heckl, and G. B. Petersen, Origins Life Evol. Biosphere **30**, 81 (2000).

[24] M. D. Upward, P. Moriarty, and P. H. Beton, Phys. Rev. B **56**, R1704 (1997).

[25] K. J. Wan, X. F. Lin, and J. Nogami, Phys. Rev. B **47**, 13700 (1993).

[26] S. Watanabe, M. Aono, and M. Tsukada, Phys. Rev. B **44**, 8330 (1991).

[27] J. F. Jia, R. G. Zhao, and W. S. Yang, Phys. Rev. B **48**, 18109 (1993).

[28] Y. Nakamura, Y. Kondo, J. Nakamura, and S. Watanabe, Surf. Sci. **493**, 206 (2001).

[29] P. Ordejon, E. Artacho, and J. M. Soler, Phys. Rev. B **53**, R10441 (1996).

[30] J. M. Soler, E. Artacho, J. D. Gale, A. Garcia, J. Junquera, P. Ordejon, and D. Sanchez-Portal, J. Phys.: Condens. Matter **14**, 2745 (2002).

[31] E. Artacho, D. Sanchez-Portal, P. Ordejon, A. Garcia, and J. M. Soler, Phys. Status Solidi B **215**, 809 (1999).

[32] J. P. Perdew, K. Burke, and M. Ernzerhof, Phys. Rev. Lett. **77**, 3865 (1996).

[33] S. F. Boys and F. Bernardi, Mol. Phys. **19**, 553 (1970).

[34] M. J. Butcher, J. W. Nolan, M. R. C. Hunt, P. H. Beton, L. Dunsch, P. Kuran, P. Geiorgi, and T. J. Dennis, Phys. Rev. B **64**, 195401 (2001).

[35] S. J. Sowerby, W. M. Heckl, and G. B. Petersen, J. Mol. Evol. **43**, 419 (1996).